Self-assembly, tunable hydrogel properties and selective anti-cancer activity of a carnosine-derived lipidated peptide

ACS APPLIED MATERIALS & INTERFACES

Research Article

Cite This: ACS Appl. Mater. Interfaces 2019, 11, 33573−33580

www.acsami.org

Self-Assembly, Tunable Hydrogel Properties, and Selective Anti-Cancer Activity of a Carnosine-Derived Lipidated Peptide

Valeria Castelletto,*[,†] Charlotte J. C. Edwards-Gayle,[†] Francesca Greco,[†] Ian W. Hamley,*[,†] Jani Seitsonen,[‡] and Janne Ruokolainen[‡]

[†]School of Chemistry, Pharmacy and Food Biosciences, University of Reading, Reading RG6 6AD, U.K.

[‡]Nanomicroscopy Center, Aalto University, Puumiehenkuja 2, Espoo FIN-02150, Finland

Supporting Information

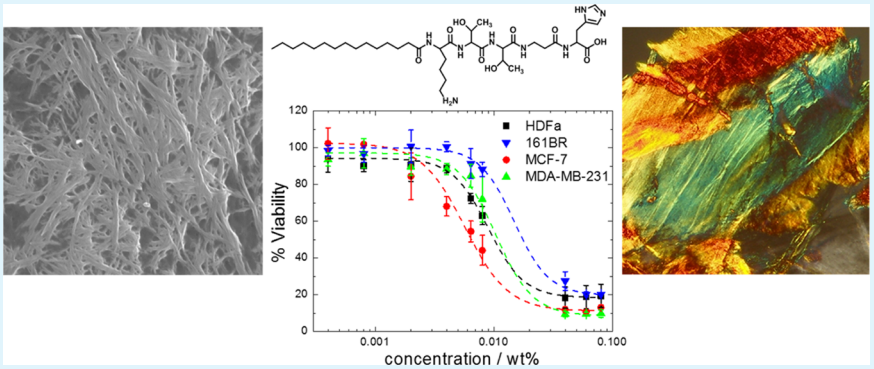

ABSTRACT: A novel lipopeptide C_{16}KTTβAH was designed that incorporates the KTT tripeptide sequence from "Matrixyl" lipopeptides along with the bioactive βAH (β-alanine-histidine) carnosine dipeptide motif, attached to a C_{16} hexadecyl lipid chain. We show that this peptide amphiphile self-assembles above a critical aggregation concentration into β-sheet nanotape structures in water, phosphate-buffered saline (PBS), and cell culture media. Nanotape bundle structures were imaged in PBS, the bundling resulting from nanotape associations because of charge screening in the buffer. In addition, hydrogelation was observed and the gel modulus was measured in different aqueous media conditions, revealing tunable hydrogel modulus depending on the concentration and nature of the aqueous phase. Stiff hydrogels were observed by direct dissolution in PBS, and it was also possible to prepare hydrogels with unprecedented high modulus from low-concentration solutions by injection of dilute aqueous solutions into PBS. These hydrogels have exceptional stiffness compared to previously reported β-sheet peptide-based materials. In addition, macroscopic soft threads which contain aligned nematic structures can be drawn from concentrated aqueous solutions of the lipopeptides. The anti-cancer activity of the lipopeptide was assessed using two model breast cancer cell lines compared to two fibroblast cell line controls. These studies revealed selective concentration-dependent cytotoxicity against MCF-7 cancer cells in the mM concentration range. It was shown that this occurs below the onset of lipopeptide aggregation (i.e., below the critical aggregation concentration), indicating that the cytotoxicity is not related to self-assembly but is an intrinsic property of C_{16}KTTβAH. Finally, hydrogels of this lipopeptide demonstrated slow uptake and release of the Congo red dye, a model diagnostic compound.

KEYWORDS: *lipopeptide, peptide amphiphile, self-assembly, hydrogel, anti-cancer*

INTRODUCTION

Lipopeptides, one type of peptide amphiphile, are attracting great interest as self-assembling biomolecules. These molecules combine designed or bio-derived/bio-inspired peptide sequences with hydrophobic lipid chains. The tendency of lipid chains to segregate from water leads to self-assembly in aqueous solution.[1−8] The self-assembled nanostructures formed, commonly nanofibrils or nanotapes (although micelles have also been observed[9]), present the peptide motif at high density, so-called multivalent display, leading to enhanced bioactivity compared to unassociated peptide molecules.[9−13]

In previous work, our group has investigated the self-assembly of lipopeptide C_{16}-KTTKS, which is a commercial Matrixyl material, used in skincare preparations.[14] We showed that it forms highly extended (up to microns) nanotape structures in aqueous solution.[15] The KTTKS sequence is derived from the procollagen I peptide[16] and this lipopeptide has collagen-stimulating properties, exemplified by studies using fibroblast cell models,[17] building on the original demonstration of extracellular matrix (ECM) (collagen and fibronectin) production of the constituent KTTKS peptide.[16] In fact, lipopeptides incorporating even shorter sequences such

Received: May 28, 2019
Accepted: August 13, 2019
Published: August 13, 2019

as C_{16}-KT are of commercial interest for cosmetic formulations, and in a previous paper, we compared the self-assembly of commercial grade C_{16}-KT with C_{16}-KTTKS and C_{16}-GHK.[18]

In other works, we examined the self-assembly of lipopeptide C_{16}-βAH incorporating the bioactive carnosine βAH (β-alanine-histidine) motif. This molecule is extensively present in vivo and has antioxidant and other properties, partly because of the metal binding capability of the histidine residue.[19,20] This lipopeptide was found to self-assemble into nanotapes, with either monolayer or bilayer packing, the bilayers being dehydrated with increasing lipopeptide concentration in water.[21] This molecule also induced thinning of phospholipid vesicles.[21] We also designed Fmoc–βAH with the aromatic Fmoc [*N*-(fluorenyl-9-methoxycarbonyl)] motif incorporated to drive self-assembly via π-stacking.[22] This molecule forms amyloid-like fibrils above a critical aggregation concentration (cac), and zinc binding of the terminal histidine residue was shown to influence the fibril morphology (and to cause gelation under defined conditions).[21]

We reasoned that a combination of the KTT peptide sequence along with βAH would potentially have synergistic bioactivity, reducing cytotoxicity to noncancerous cells. Thus, we designed the novel lipopeptide C_{16}KTTβAH (Supporting Information Scheme S1) and herein investigate its self-assembly and cytotoxicity toward fibroblasts and two breast cancer cell lines. In addition, it is known that carnosine has anti-cancer activity,[23,24] and the β-alanine constituent of carnosine has activity against breast cancer.[25] We hypothesized that the anti-cancer activity may relate to self-assembly properties of the lipopeptide because lipopeptides may form extended networks of nanofibril structures resembling an ECM and self-assembled structures present active peptides at high density. It is known that the ECM plays an important role in cancer metastasis, especially with the involvement of matrix metalloproteases including collagenases.[26−28] On the other hand, considering amyloid peptides such as Amyloid β, self-assembly into fibrils can remove toxic oligomers and monomers from the solution.[29] In fact, our results indicate that the observed selective concentration-dependent anti-cancer activity is not correlated with the concentration at which self-assembly occurs (the critical aggregation concentration), and is an inherent property of the lipopeptide. We also investigate the tunable hydrogelation properties uncovered for this novel lipopeptide and present a method to prepare a hydrogel at relatively low peptide concentration, by injection of an aqueous solution into the buffer. In addition, it was possible to draw macroscopic soft fibers from concentrated aqueous solutions, which have a nematic texture. This lipopeptide has a remarkable combination of mechanical properties and anti-cancer activity.

EXPERIMENTAL SECTION

Materials. The lipidated peptide C_{16}KTTβAH was purchased from CS Bio (Menlo Park, California) and supplied as the trifluoroacetate (TFA) salt. Purity was 98.19% by analytical high-performance liquid chromatography (HPLC) using acetonitrile (0.1% TFA)/water (0.1% TFA) gradient. The molar mass measured by electrospray ionization (ESI)–mass spectrometry (MS) was 795 g mol^{-1} (795.02 g mol^{-1} expected). Elemental analysis of CHN and O was performed by combustion and pyrolysis using a Thermo FlashEA 1112 instrument and F analysis by ion chromatography using a Metrohm 761 Compact Ion Chromatograph following oxygen flask combustion of the sample. These measurements provided C 50.78%, H 5.18%, N 11.64%, O 21.09%, and F 2.96%, consistent with the presence of TFA salt. Scheme S1 shows the chemical structure of C_{16}KTTβAH and Figure S1 contains the HPLC and ESI–MS spectra. Solutions of peptides were prepared by mixing weighed amounts of water and peptide or phosphate-buffered saline (PBS) and peptide. The native pH of the lipopeptide in water was found to be 6. The mixtures were left to equilibrate for 24 h before characterization. The solvent used to prepare the solution is only indicated for samples dissolved in PBS.

Hydrogel Formation. Hard gels were obtained by mixing 1–5 wt % C_{16}KTTβAH in PBS, while 1 wt % C_{16}KTTβAH in water provided a soft gel. In an attempt to form a low-concentration hydrogel starting from an aqueous solution, 2 mL of PBS was loaded onto a Petri dish, and then 0.5 mL of 0.1 wt % C_{16}KTTβAH in water was injected into the PBS solution. A hydrogel was spontaneously formed after a few seconds, and the excess of PBS was removed from the Petri dish. The formed hydrogel was recovered and placed inside an Eppendorf. The procedure was repeated several times until a total of 6 mL of 0.1 wt % C_{16}KTTβAH aqueous solution was injected in the PBS, making a total of 0.75 mL of hydrogel. The concentration of the lipopeptide in the hydrogel was estimated to be ~0.8 wt % C_{16}KTTβAH, based on the yield of the hydrogel produced (6 mL of injected 0.1 wt % sol produced 0.75 mL of hydrogel).

Circular Dichroism Spectroscopy. Circular dichroism (CD) spectra were recorded as described previously.[30] The CD signal from the water was subtracted from the CD data for samples in aqueous solution as background, or in the case of measurements in media, the spectrum from media was subtracted.

Fourier Transform Infrared Spectroscopy. Spectra were recorded as described previously.[30]

X-ray Diffraction. Measurements were performed as described previously.[30]

Rheology. The dynamic shear moduli were measured as described previously.[30]

Transmission Electron Microscopy. Transmission electron microscopy (TEM) imaging was performed as described previously.[30]

Cryogenic TEM. Imaging was carried out as described previously.[30]

Scanning Electron Microscopy. The hydrogel was freeze-dried and placed on a stub covered with a carbon tab (Agar Scientific, UK) and then coated with gold for 2–3 min and imaged as described previously.[31]

Small-Angle X-ray Scattering. Synchrotron small-angle X-ray scattering (SAXS) experiments on solutions were performed on beam line B21 at Diamond (Didcot, UK) and on ID02 (ESRF, France), as described previously.[30]

Fluorescence Assays. The critical aggregation concentration (cac) was determined via thioflavin T (ThT) or pyrene fluorescence assays, as described previously.[30]

For the pyrene assays, a dried film of pyrene (Pyr) was obtained by evaporating a solution containing 0.02 wt % Pyr in ethanol. The Pyr dried film was then resuspended in DMEM [without fetal bovine serum (FBS) or antimycotic–antibiotic supplements] to give a 3×10^{-5} wt % Pyr solution. C_{16}KTTβAH solutions containing 9×10^{-4} to 0.02 wt % lipopeptide were prepared using 3×10^{-5} wt % Pyr in DMEM as a solvent. Pyr fluorescence emission spectra were recorded from 360 to 460 nm, using λ_{ex} = 339 nm. The spectra for 3×10^{-5} wt % Pyr in DMEM were subtracted from the spectra of solutions containing Pyr and C_{16}KTTβAH. Experiments were performed at 37 °C.

Dye Uptake and Release Studies. Uptake of Congo red was measured by immersing 100 μL of 1 wt % C_{16}KTTβAH in PBS in 2 mL of 5×10^{-3} wt % Congo red solution in PBS. To measure dye release from a 1 wt % C_{16}KTTβAH hydrogel in PBS, 100 μL of hydrogel was loaded with 5×10^{-3} wt % Congo red solution. The hydrogel was then immersed in 2 mL of PBS solution. UV–vis spectra to monitor uptake and release were obtained by taking aliquots of solution and measuring spectra using a Varian Cary 300 Bio UV/vis spectrometer, recording the absorbance maximum at λ = 498 nm at selected time intervals.

DOI: 10.1021/acsami.9b09065
ACS Appl. Mater. Interfaces 2019, 11, 33573–33580

Polarized Optical Microscopy. A C_{16}KTTβAH hydrogel was first stained using a freshly prepared 10^{-3} wt % Congo red solution. Images were collected as described previously.[31]

Cytotoxicity Assays. The cytotoxicity of C_{16}KTTβAH was examined using a MTT [3-(4,5-dimethylthiazol-2-yl)-2,5-diphenyltetrazolium bromide] assay. In vitro assays were performed with the human skin fibroblast cell line, 161BR (European Collection of Authenticated Cell Cultures, (ECACC) 90011810), human breast adenocarcinoma cell line MCF-7 (ECACC 86012803), human breast adenocarcinoma MDMA-MB-231 (ECACC 92020424), or primary human dermal fibroblasts, HDFa (Gibco).

161Br cells were cultured in MEME (Minimum Essential Medium Eagle), 2 mM glutamine, enriched with 15% FBS, 1% nonessential amino acids, and 1% antimycotic−antibiotic. MCF-7 cells were cultured in Gibco RPMI 1640 Medium enriched with 15% FBS and 1% antimycotic−antibiotic. MDMA-MB-231 cells were cultured in DMEM (Dulbecco's Modified Essential Medium) enriched with 10% FBS and 1% antimycotic−antibiotic. All cells were maintained in a humidified atmosphere at 37 °C and 5% CO_2.

The same protocol, detailed as follows, was used for MTT assays on cell cultures with 161Br, MCF-7, MDMA-MB, or HDFa. MCF-7, HDFa, and 161BR cells were seeded into a 96-well plate at a concentration of 4×10^4 cells/mL, and MDMA-MB-231 was plated at a concentration of 2×10^4 cells/mL. All cells were left to adhere for 24 h in 100 μL of complete medium. C_{16}KTTβAH was dissolved in complete medium and added to the cells to give a final volume of 200 μL at concentrations between 0.001 and 0.1 wt %. One well, containing 200 μL of complete medium with no peptide, was used as the negative control. Then, the cells were incubated for 19 h. After this, 20 μL of MTT (5 mg/mL, in PBS) was added to each well plate and allowed to incubate for 5 h (24 h total). Formazan UV absorbance was measured as described previously.[30] MTT assays were performed in triplicate, except MCF-7, which was performed as five separate measurements.

To assess the cell viability of the hydrogels, an MTT assay was used. First, the hydrogel stability was tested in 96-well plates to ensure whether the hydrogel stayed intact for 24 h in the media. Both the 1 wt % gel and the hydrogel prepared by injecting a 0.1 wt % aqueous solution in PBS were found to be stable. Following this, both types of hydrogel were spread onto the bottom of a 96-well plate, and MDA-MB-231, MCF-7, or HDFa cells were seeded on the top of the gels at 4×10^4 cells/mL. Control solutions of cells alone in media and hydrogels alone in media were also prepared. After 19 h, 20 μL of MTT solution (5 mg/mL in PBS) was added and incubated for 5 h. Following this, the supernatant was removed and 100 μL of dimethyl sulfoxide added to dissolve the formazan crystals. Plates were then incubated for 30 min and read using a UV plate microreader (λ = 570 nm), and the results are reported as 100 × (hydrogel + cell absorbance − hydrogel only absorbance)/(absorbance of cells alone in media).

RESULTS AND DISCUSSION

We first examined the conformation and self-assembly of C_{16}KTTβAH in water, including potential hydrogel formation. The cytotoxicity of C_{16}KTTβAH was then investigated against two different breast cancer cell lines compared to fibroblast cell controls.

Conformation and Self-Assembly in Solution. The conformation and self-assembly of C_{16}KTTβAH were investigated in water, performing fluorescence spectroscopy assays and CD, Fourier transform infrared (FTIR), X-ray diffraction (XRD), SAXS, wide-angle X-ray scattering, cryogenic TEM (cryo-TEM), and rheology experiments. The results are summarized in Figures 1 and 2. We used the dye ThT to determine the existence and location of the critical aggregation concentration (cac). This dye is sensitive to the formation of amyloid fibrils.[32,33] The concentration-dependent ThT fluorescence shown in Figure 1a reveals a cac = (0.014 ± 0.002) wt % (the data are presented with the concentration on a linear scale, as shown in Supporting Information Figure S2, which shows the same cac transition). A cac assay was also performed using pyrene as a fluorescent probe. The data (as shown in Supporting Information Figure S2) indicate a cac = (0.017 ± 0.002) wt %, which is consistent with that obtained using ThT. CD spectra are shown in Figure 1b, which display the characteristics of a β-sheet secondary structure above the cac, with a characteristic positive maximum near 190 nm and a negative minimum at 216 nm.[34−36] This conclusion is supported by analysis of the FTIR spectra in the amide I′ region shown in Figure 1c. A peak characteristic of β-sheet structure[37−39] at 1628 cm^{-1} is clearly present for samples with 0.5 and 1 wt % peptide (and present as a shoulder at 0.05 wt % peptide) above the cac, along with a peak at 1610 cm^{-1} due to

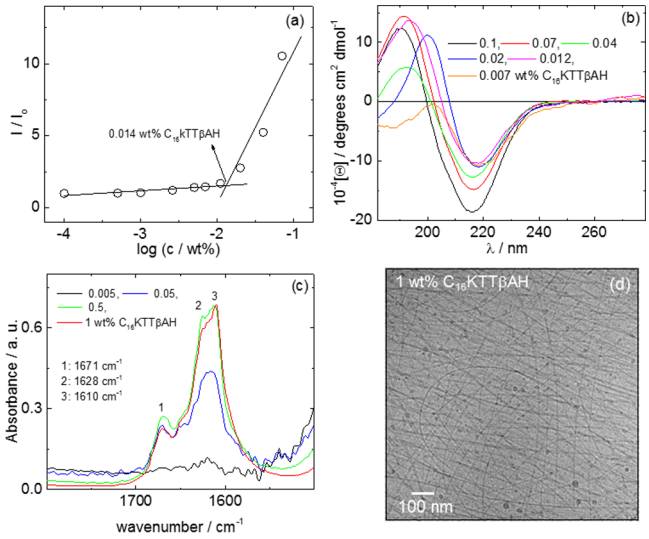

Figure 1. (a) ThT assay to determine the critical aggregation concentration for C_{16}KTTβAH in water. Characterization of C_{16}KTTβAH in water: (b) CD spectra, (c) FTIR spectra, and (d) cryo-TEM image.

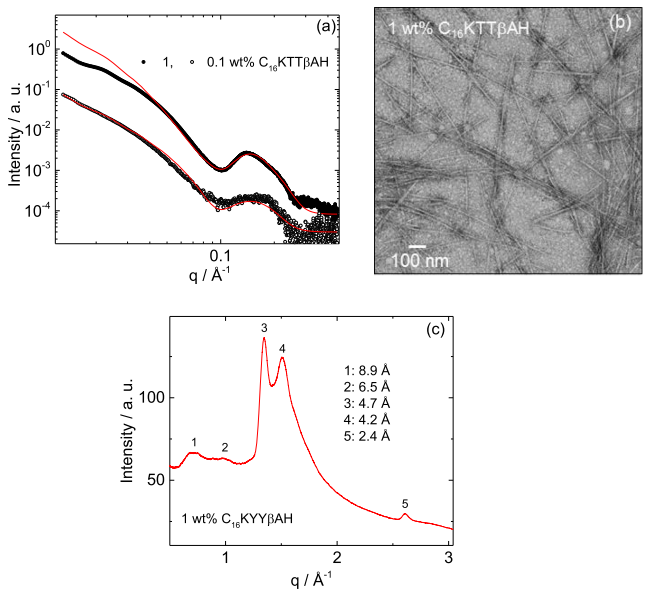

Figure 2. Self-assembly of C_{16}KTTβAH in water: (a) SAXS data, (b) TEM image, and (c) fiber XRD profile. The full lines in (a) correspond to the fitting of the SAXS data.

DOI: 10.1021/acsami.9b09065
ACS Appl. Mater. Interfaces 2019, 11, 33573−33580

histidine vibrational modes.[21,40] The peak at 1672 cm^{-1} is due to bound TFA counterions.[30] The cryo-TEM image shown in Figure 1d clearly reveals the presence of nanotape (or nanofiber bundle) structures in a 1 wt % solution of C_{16}KTTβAH, with regions of twisting of the nanotapes visible.

Figure 2 contains data from additional measurements to probe the conformation and assembly of C_{16}KTTβAH in water. The SAXS intensity profiles shown in Figure 2a measured at two concentrations above the cac reveal the form factor shapes which were fitted using a model for lipopeptide bilayers[41,42] (based on a model for lipid bilayers[43]), consistent with the nanotape structures observed by TEM. The fit parameters are listed in Supporting Information Table S1. The TEM image for a sample dried from a 1 wt % solution shown in Figure 2b shows nanotape (or nanofibril bundle) structures, consistent with the cryo-TEM image in Figure 1d. Fiber XRD was performed to determine the secondary structure of the peptide, and the XRD intensity profile shown in Figure 2c confirms a β-sheet structure because peaks are observed corresponding to a "cross-β" XRD pattern[44,45] with spacings d = 4.7 Å (β-strand spacing) and 8.9 Å (β-sheet spacing). The d = 6.5 Å peak and d = 4.2 Å peak are assigned to intra-sheet packing and lipid chain packing (in a fraction of non-β-sheet assemblies) distances, respectively, and the d = 2.4 Å peak is assigned to intra-lipid or intra-peptide periodicity. The "cross-β" pattern was confirmed in two-dimensional (2D) aligned fiber XRD patterns (an example is shown in Supporting Information Figure S4).

We reasoned that self-assembly and hydrogelation could be tuned by the use of suitable buffer conditions. We thus investigated the conformation and aggregation of C_{16}KTTβAH in PBS. Figure 3 contains data measured in PBS solutions from SAXS, cryo-TEM, and XRD analyses. The SAXS intensity profiles measured at several concentrations shown in Figure 3a have similar shape (low q scaling and broad form factor maximum at high q) to those observed for the nanotapes in water (Figure 2a) and were fitted with a similar model (the bilayer form factor fit parameters are provided in Supporting Information Table S1). The cryo-TEM image shown in Figure 3b shows a distinct morphology to that observed in water (Figures 1d and 2b) because bundling of nanotapes is evident, producing raft-like assemblies. The nanotape bundling is presumably facilitated by reduced electrostatic repulsion between peptide-charged residues because of screening in the buffer. The XRD pattern shown in Figure 3c confirms a β-sheet structure because of the presence of d = 4.7 Å and d = 8.5/16.5 Å "cross-β" pattern spacings. The d = 4.1 Å peak is compatible with local lipid chain intermolecular packing. The shorter d-spacing peaks observed are due to intra-lipopeptide molecular spacings. In summary, the β-sheet nanotape structure is retained in PBS, with the additional feature of nanotape bundling. These properties suggested the potential for hydrogel formation, which was thoroughly examined.

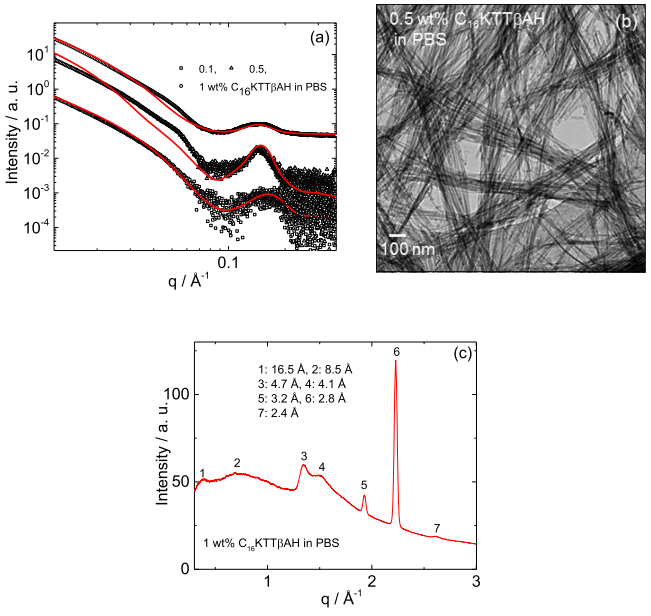

Figure 3. Self-assembly of C_{16}KTTβAH in PBS. (a) SAXS profiles, (b) cryo-TEM image, and (d) XRD data. The inset in (c) shows the corresponding 2D XRD pattern. The full lines in (a) correspond to the fitting of the SAXS data.

Hydrogel Formation. Hard gel formation was observed in PBS (in the concentration range of 1−5 wt % examined), while in water, C_{16}KTTβAH formed a soft gel at 1 wt % concentration. Remarkably, it is possible to prepare a low-concentration hydrogel starting from an aqueous solution by injecting a dilute (0.1 wt %) solution of C_{16}KTTβAH in water into PBS solution. Figure 4a shows a scanning electron microscopy (SEM) micrograph which reveals the fibrillar network structure within a gel formed by injecting into PBS solution. This hydrogel is able to bind Congo red, which is a diagnostic dye for amyloid fibril formation, leading to green birefringence textures in the polarized optical microscope.[45] A representative image is presented in Figure 4b. The dynamic mechanical properties of the hydrogels were measured using shear rheometry. Figure 4c contains selected data showing the frequency dependence of the storage modulus G'. The full set of frequency sweep data (including G'') along with stress sweep data, used to determine the linear viscoelastic regime, is

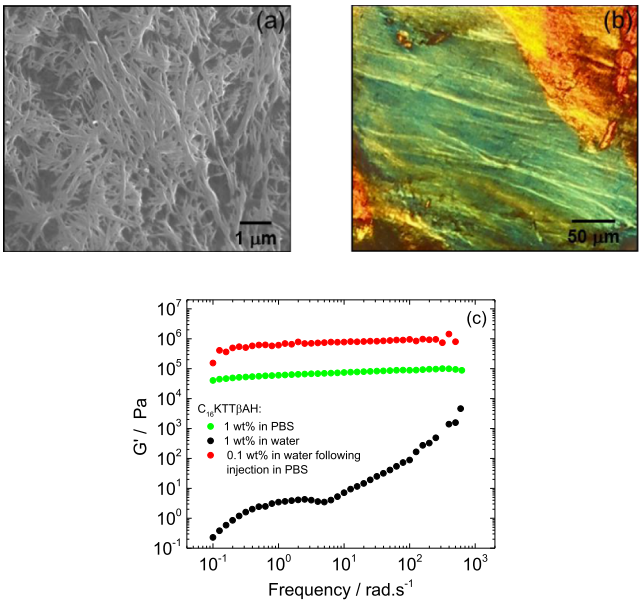

Figure 4. Characterization of 0.1 wt % C_{16}KTTβAH in water following injection in PBS: (a) SEM image and (b) Congo red birefringence observed by POM. (c) Storage modulus, G', measured for 1 and 5 wt % C_{16}KTTβAH in PBS, 1 wt % C_{16}KTTβAH in water, and 0.1 wt % C_{16}KTTβAH in water following injection in PBS.

DOI: 10.1021/acsami.9b09065
ACS Appl. Mater. Interfaces 2019, 11, 33573−33580

shown in Supporting Information Figure S5. The data in Figure 4c show that the gel from the peptide dissolved in water has soft gel characteristics, with a strongly frequency-dependent modulus which has low magnitude at low frequency. In contrast, the storage modulus for the 1 wt % PBS gel is largely independent of frequency and has a value G' = 50−100 kPa (depending on frequency), corresponding to a stiff hydrogel. The highest modulus is recorded for the gel prepared by injecting an aqueous solution into PBS solution, with G' = 0.5−1 MPa, depending weakly on frequency. This is exceptionally high compared to the modulus reported for the majority of β-sheet peptide-based systems,[46−50] although a modulus approaching this value has been reported for peptide FEFK, undergoing reverse hydrolysis at high concentration in the presence of a protease.[51] We also noted that it was possible to draw macroscopic fiber from more concentrated aqueous solutions of C_{16}KTTβAH as shown in Figure 5. The fibers

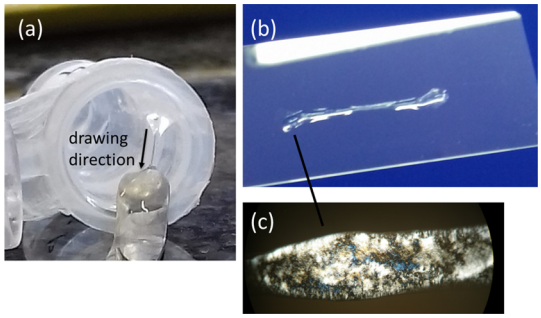

Figure 5. (a,b) Threads formed by drawing C_{16}KTTβAH from a 5 wt % aqueous solution, manual drawing direction shown in part (a) and (c) polarized optical microscope showing nematic texture within a thread.

have a nematic texture as confirmed by polarized optical microscopy (POM) (Figure 5c). This indicates that they comprise an aligned structure, which is presumably an aligned network of nanotape structures. The fact that threads can be drawn points to sufficient extensional modulus of the material (although the fibers are too soft and fluidic to quantify this by tensile rheometry). We note that the samples in the rheometer were not macroscopically aligned (unlike the drawn fibers), and therefore, anisotropy in G' was not expected. In summary, hydrogels with tunable shear modulus can be obtained under appropriate formulation conditions of C_{16}KTTβAH and concentrated solutions can be drawn into aligned lipopeptide threads.

Selective Anti-Cancer Activity. To examine whether there was any significant difference in the cytotoxicity of C_{16}KTTβAH toward normal cell lines and breast cancer cell lines, an MTT mitochondrial activity assay was carried out. The results are shown in Figure 6. Cancer cell lines MCF-7 and MDA-MB-231 were selected as two models of breast cancer.[52−54] The MCF-7 cell line expresses estrogen and progesterone receptors, it induces MMP-2 (collagenase) activation,[55−57] and is more responsive to chemotherapy.[54] MDA-MB-231 does not express estrogen and progesterone receptors[52−54] and is a triple negative cell line, with an intermediate response to chemotherapy, making it a "tougher" cell line. The 161BR continuous fibroblast cell line and HDFa primary human dermal fibroblast cell lines were used as controls.

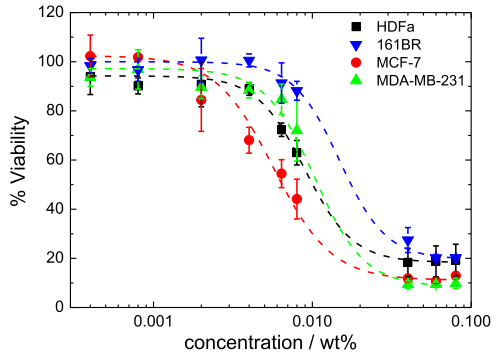

Figure 6. Cytotoxicity profiles for C_{16}KTTβAH against the cell lines indicated including MCF-7 and MDA-MB-231 breast cancer cells and HDFa and 161BR fibroblasts.

The IC50 values determined from the MTT assay results (Table 1) indicate that the cytotoxicity of C_{16}KTTβAH is

Table 1. IC50 Values

cell line	IC50/wt %
161BR	0.0174 ± 0.0059
HDFa	0.00955 ± 0.0013
MCF-7	0.0065 ± 0.0010
MDA-MB-231	0.0107 ± 0.0014

greatest for the MCF-7 cell line at concentrations above 0.002 wt %. The cytotoxicity (at a given concentration above 0.002 wt %) then decreases in the order HDFa > MDA-MB-231 > 161BR. The IC50 values suggest that the two cancer cell lines are more susceptible to C_{16}KTTβAH than 161BR fibroblasts. To further examine this, statistical significance was examined using analysis of variance, which revealed significant differences in the cytotoxicity values for MCF-7 and control cell line 161BR within the concentration range of 0.004−0.08 wt %. Moreover, there is a statistical significance between the MDA-MB-231 and 161BR cytotoxicity at concentrations 0.004, 0.04, and 0.06 wt %. There is also a difference between the cytotoxicity toward 161BR and HDFa cells, which may be because the latter cell line is a primary cell line, whereas the former is a continuous cell line. There are no significant differences between cytotoxicity toward HDFa and the cancer cell lines, although the IC50 value for MCF-7 is 0.003 wt % lower than for HDFa.

Additional cytotoxicity studies were performed on the gels. Gels were found (by visual inspection) to be stable in media (both 1 wt % gels in PBS or hydrogels prepared by injecting a dilute aqueous solution into water). The cytotoxicity assay results obtained using MCF-7, MDA-MB-231, and HDFa cell lines, as used for the assays on solutions, are shown in Supporting Information Figure S6. These show that the 1 wt % C_{16}KTTβAH in PBS hydrogel shows higher cytotoxicity against the two cancer cell lines than HDFa, although the hydrogel prepared by injection of a 0.1 wt % aqueous solution in PBS unexpectedly shows higher cytotoxicity toward HDFa cells.

Aggregation State in Media. To assess aggregation and conformation of the peptide under media conditions similar to those for cell culture (the same basal media but without FBS, which can interfere with fluorescence and CD measurements), fluorescence cac assays, CD, TEM, and SAXS were performed. The cac was assayed using pyrene, as it is probe sensitive to

DOI: 10.1021/acsami.9b09065
ACS Appl. Mater. Interfaces 2019, 11, 33573−33580

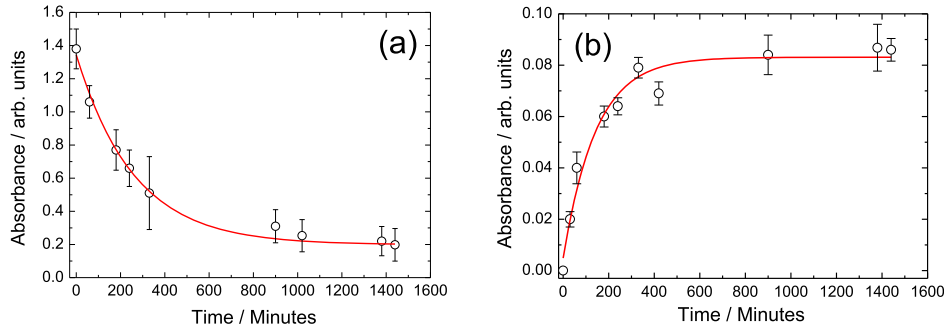

Figure 7. (a) Uptake and (b) release of Congo red by a 1 wt % hydrogel of C_{16}KTTβAH in PBS.

aggregation driven by segregation of hydrophobic regions of molecules from the aqueous phase[58,59] (the ThT assay was not successful in media). The fluorescence spectra obtained at 37 °C along with plots of the concentration dependence of the I_{373} vibronic band intensity are shown in Supporting Information Figure S7. The cac is found at (0.01 ± 0.005) wt %, which is the same as that in water, within uncertainty. The CD spectra measured at 37 °C shown in Supporting Information Figure S8a confirm the presence of β-sheet structures above the cac while SAXS intensity profiles presented in Supporting Information Figure S8b are consistent with nanotape structures, having similar shapes (and q scalings) to those shown in Figures 2a and 3a. Nanotape structures are also clearly revealed by TEM (Supporting Information Figure S8c). In summary, these spectroscopic, microscopic, and scattering measurements confirm that C_{16}KTTβAH is aggregated into β-sheet structures in cell culture media above the same cac as observed in water. However, the onset of cytotoxicity is observed for all cell lines at concentrations substantially below the cac (Figure 6).

Dye Uptake and Release from Hydrogels. As a simple model for a diagnostic/drug-like compound, the uptake and release of the fluorescent dye Congo red, which is mentioned above, is used to test for the presence of amyloid. A hydrogel was prepared with 1 wt % C_{16}KTTβAH in PBS, and uptake of Congo red solution was monitored by UV absorbance. Figure 7a shows that the hydrogel is able to slowly uptake the dye from the solution, causing a reduction in the absorbance of the dye in the solution, saturating after approximately 10 h. Images of the initial and final (after 24 h) states of solution and gel are shown in Supporting Information Figure S9. The hydrogel is able to slowly release the dye, after the dye-loaded gel is placed into a fresh PBS solution. Figure 7b shows the corresponding absorbance measurements for the free dye in solution. The release occurs over a similar time scale to the uptake, saturating after about 10 h. Cumulative uptake and release plots are included as the Supporting Information, Figure S10. These results show that the C_{16}KTTβAH gels are suited for slow release applications of diagnostic molecules.

CONCLUSIONS

In summary, C_{16}KTTβAH self-assembles into nanotape structures above a critical aggregation concentration in aqueous solution. In PBS, the nanotapes pack side-by-side into raft-like bundles (because of the screening of electrostatic repulsions on the charged cationic residues and C terminus). The nanotapes are characterized by a β-sheet secondary structure. The same structures are retained under the conditions of the cell culture media used for the cytotoxicity assays.

The modulus of the hydrogels is enhanced by the use of PBS, presumably because of the screening of repulsive electrostatic interactions of K (and H at sufficiently low pH) residues and charge on the C terminus. Furthermore, the modulus can be tuned over a considerable range (from less than 1 kPa to 1 MPa) depending on the type of buffer and preparation method. The modulus for the sample obtained by injection of a dilute water solution of peptide into PBS is higher than that for a higher concentration of peptide dissolved directly in PBS, which points to the likely role of interface effects on the structuring of the gel which forms upon injection. Stupp's group has suggested that self-assembly starts from the interface when injecting peptide amphiphiles into salt solutions because of interfacial charge screening.[60] We propose that a similar mechanism (enhanced assembly of a nanotape network at the interface) is likely to operate for C_{16}KTTβAH injected into PBS. The role of charge screening on peptide fibril bundling and network formation, leading to hydrogelation, has previously been investigated for model peptides such as FEFEFKFK[61] or FEFK, which, as mentioned above, undergoes enzyme-triggered hydrogelation due to reverse hydrolysis (which leads to the formation of octapeptides such as FEFEFKFK and FEFKFEFK, which are believed to be responsible for the observed gelation).[51]

The observed range of moduli of hydrogels of C_{16}KTTβAH corresponds to a range of gel stiffness of interest in tissue engineering because stem cell differentiation into different phenotypes has been shown to depend on matrix (hydrogel) modulus.[62] The modulus approaching 1 MPa of the hydrogel prepared by injection in PBS is extremely high for a self-assembled material, which is more typical of polymeric or cross-linked materials. In addition, fibers can be drawn from aqueous solutions, and these membrane-like structures clearly have sufficient extensional modulus to be drawn into macroscopic fibers, with a nematic texture resulting from an aligned nanotape network. Thus, the lipopeptide C_{16}KTTβAH possesses an excellent combination of shear and extensional mechanical properties depending on the processing conditions. This suggests great potential in future applications in cell culture, tissue engineering, and regenerative medicine, for example. In addition, we have shown that hydrogels prepared from C_{16}KTTβAH are able to steadily release a model dye compound and thus show promise for slow release applications of diagnostic, and potentially therapeutic, compounds. The model dye compound Congo red that shows slow uptake and release properties is employed as a diagnostic compound for amyloid formation (and was used as such by us, Figure 4b),

DOI: 10.1021/acsami.9b09065
ACS Appl. Mater. Interfaces 2019, 11, 33573−33580

which may enhance the binding facilitating slow release. Future work should examine the release of other dyes (with different charge and binding interactions) or, for example, model therapeutic anticancer compounds. Gels with slow release properties of actives are expected to be particularly useful for topical application.

The cytotoxicity assays show that C_{16}KTTβAH selectively kills MCF-7 breast cancer cells compared to fibroblasts in a mM concentration range (the IC50 value corresponds to 82 mM). The cell viability begins to decrease nearly 1 order of magnitude in concentration below the cac, and indeed almost complete cytotoxicity is observed just above the cac. These observations indicate that cytotoxicity is not correlated with the formation of β-sheet nanotape assemblies but is an intrinsic property of the lipopeptide. However, selective anticancer activity against MCF-7 cells is also observed for the (β-sheet fibrillar) 1 wt % C_{16}KTTβAH in PBS hydrogel.

Our findings suggest that C_{16}KTTβAH is a promising candidate for further studies as a potential therapeutic agent to treat breast cancer. It is also of considerable interest to examine its activity against other types of cancers, as well as elucidating its mode of activity. In addition, this lipopeptide has a remarkable range of tunable hydrogel properties and can be drawn into stretchable fibers, based on a nematic network structure.

■ ASSOCIATED CONTENT

Supporting Information

The Supporting Information is available free of charge on the ACS Publications website at DOI: 10.1021/acsami.9b09065.

Method to fit SAXS data, parameters obtained from SAXS data fittings, scheme of molecular structure, HPLC and ESI−MS spectra, fluorescence data, fiber XRD pattern, rheology results, and results from characterization of self-assembly in media (PDF)

■ AUTHOR INFORMATION

Corresponding Authors

*E-mail: V.Castelletto@reading.ac.uk (V.C.).
*E-mail: I.W.Hamley@reading.ac.uk (I.W.H.).

ORCID

Valeria Castelletto: 0000-0002-3705-0162
Ian W. Hamley: 0000-0002-4549-0926

Notes

The authors declare no competing financial interest.

■ ACKNOWLEDGMENTS

The work of VC was supported by EPSRC Platform grant EP/L020599/1 "Nanostructured Polymeric Materials for Healthcare) to IWH. CJCEG was supported by a studentship cofunded by the University of Reading and Diamond Light Source. The authors are grateful to Diamond for beamtime on B21 (ref. SM18523-1) and to Katsuaki Inoue for support. The authors are grateful to the ESRF for beamtime on ID02 (ref. SC4739) and Alessandro Mariani for support. They thank Nick Spencer for assistance with XRD experiments. They acknowledge access to the Chemical Analysis Facility laboratory (University of Reading).

■ REFERENCES

(1) Löwik, D. W. P. M.; Van Hest, J. C. M. Peptide Based Amphiphiles. *Chem. Soc. Rev.* **2004**, *33*, 234−245.
(2) Cui, H.; Webber, M. J.; Stupp, S. I. Self-Assembly of Peptide Amphiphiles: from Molecules to Nanostructures to Biomaterials. *Biopolymers* **2010**, *94*, 1−18.
(3) Zhao, X.; Pan, F.; Xu, H.; Yaseen, M.; Shan, H.; Hauser, C. A. E.; Zhang, S.; Lu, J. R. Molecular Self-Assembly and Applications of Designer Peptide Amphiphiles. *Chem. Soc. Rev.* **2010**, *41*, 3480−3498.
(4) Versluis, F.; Marsden, H. R.; Kros, A. Power Struggles in Peptide-Amphiphile Nanostructures. *Chem. Soc. Rev.* **2010**, *39*, 3434−3444.
(5) Hamley, I. W. Self-Assembly of Amphiphilic Peptides. *Soft Matter* **2011**, *7*, 4122−4138.
(6) Dehsorkhi, A.; Castelletto, V.; Hamley, I. W. Self-Assembling Amphiphilic Peptides. *J. Pept. Sci.* **2014**, *20*, 453−467.
(7) Hamley, I. W. Lipopeptides: From Self-Assembly to Bioactivity. *Chem. Commun.* **2015**, *51*, 8574−8583.
(8) Hutchinson, J. A.; Burholt, S.; Hamley, I. W. Peptide Hormones and Lipopeptides: from Self-Assembly to Therapeutic Applications. *J. Pept. Sci.* **2017**, *23*, 82−94.
(9) Trent, A.; Marullo, R.; Lin, B.; Black, M.; Tirrell, M. Structural Properties of Soluble Peptide Amphiphile Micelles. *Soft Matter* **2011**, *7*, 9572−9582.
(10) Matson, J. B.; Stupp, S. I. Self-Assembling Peptide Scaffolds for Regenerative Medicine. *Chem. Commun.* **2012**, *48*, 26−33.
(11) Arslan, E.; Garip, I. C.; Gulseren, G.; Tekinay, A. B.; Guler, M. O. Bioactive Supramolecular Peptide Nanofibers for Regenerative Medicine. *Adv. Healthc. Mater.* **2014**, *3*, 1357−1376.
(12) Hendricks, M. P.; Sato, K.; Palmer, L. C.; Stupp, S. I. Supramolecular Assembly of Peptide Amphiphiles. *Accounts Chem. Res.* **2017**, *50*, 2440−2448.
(13) Sato, K.; Hendricks, M. P.; Palmer, L. C.; Stupp, S. I. Peptide Supramolecular Materials for Therapeutics. *Chem. Soc. Rev.* **2018**, *47*, 7539−7551.
(14) Lintner, K.; Peschard, O. Biologically Active Peptides: From s Laboratory Bench Curiosity to s Functional Skin Care Product. *Int. J. Cosmet. Sci.* **2000**, *22*, 207−218.
(15) Castelletto, V.; Hamley, I. W.; Perez, J.; Abezgauz, L.; Danino, D. Fibrillar Superstructure from Extended Nanotapes Formed by a Collagen-Stimulating Peptide. *Chem. Commun.* **2010**, *46*, 9185−9187.
(16) Katayama, K.; Armendariz-Borunda, J.; Raghow, R.; Kang, A. H.; Seyer, J. M. A Pentapeptide From Type-I Procollagen Promotes Extracellular-Matrix Production. *J. Biol. Chem.* **1993**, *268*, 9941−9944.
(17) Jones, R. R.; Castelletto, V.; Connon, C. J.; Hamley, I. W. Collagen Stimulating Effect Of Peptide Amphiphile C_{16}−KTTKS on Human Fibroblasts. *Mol. Pharmaceutics* **2013**, *10*, 1063−1069.
(18) Castelletto, V.; Hamley, I. W.; Whitehouse, C.; Matts, P. J.; Osborne, R.; Baker, E. S. Self-Assembly of Palmitoyl Lipopeptides used in Skin Care Products. *Langmuir* **2013**, *29*, 9149−9155.
(19) Gariballa, S.; Sinclair, A. J. Carnosine: Physiological Properties and Therapeutic Potential. *Age Ageing* **2000**, *29*, 207−210.
(20) Bonfanti, L.; Peretto, P.; De Marchis, S.; Fasolo, A. Carnosine-Related Dipeptides in The Mammalian Brain. *Prog. Neurobiol.* **1999**, *59*, 333−353.
(21) Castelletto, V.; Cheng, G.; Stain, C.; Connon, C. J.; Hamley, I. W. Self-Assembly of a Peptide Amphiphile Containing L-Carnosine and its Mixtures with a Multilamellar Vesicle Forming Lipid. *Langmuir* **2012**, *28*, 11599−11608.
(22) Castelletto, V.; Cheng, G.; Greenland, B. W.; Hamley, I. W.; Harris, P. J. F. Tuning the Self-Assembly of the Bioactive Dipeptide L-Carnosine by Incorporation of a Bulky Aromatic Substituent. *Langmuir* **2011**, *27*, 2980−2988.
(23) Gaunitz, F.; Hipkiss, A. R. Carnosine and Cancer: A Perspective. *Amino Acids* **2012**, *43*, 135−142.
(24) Iovine, B.; Oliviero, G.; Garofalo, M.; Orefice, M.; Nocella, F.; Borbone, N.; Piccialli, V.; Centore, R.; Mazzone, M.; Piccialli, G.; Bevilacqua, M. A. The Anti-Proliferative Effect of L-Carnosine Correlates with a Decreased Expression Of Hypoxia Inducible Factor

DOI: 10.1021/acsami.9b09065
ACS Appl. Mater. Interfaces 2019, 11, 33573−33580

1 Alpha in Human Colon Cancer Cells. *PLoS One* **2014**, *9*, No. e96755.
(25) Vaughan, R. A.; Gannon, N. P.; Garcia-Smith, R.; Licon-Munoz, Y.; Barberena, M. A.; Bisoffi, M.; Trujillo, K. A. β-Alanine Suppresses Malignant Breast Epithelial Cell Aggressiveness through Alterations in Metabolism and Cellular Acidity in vitro. *Mol. Cancer* **2014**, *13*, 14.
(26) Overall, C. M.; López-Otín, C. Strategies For MMP Inhibition In Cancer: Innovations for The Post-Trial Era. *Nat. Rev. Cancer* **2002**, *2*, 657−672.
(27) Rodríguez, D.; Morrison, C. J.; Overall, C. M. Matrix Metalloproteinases: What do they not do? New Substrates and Biological Roles Identified by Murine Models and Proteomics. *Biochim. Biophys. Acta Mol. Cell Res.* **2010**, *1803*, 39−54.
(28) Cathcart, J.; Pulkoski-Gross, A.; Cao, J. Targeting Matrix Metalloproteinases in Cancer: Bringing New Life to Old Ideas. *Genes Dis.* **2015**, *2*, 26−34.
(29) Hamley, I. W. The Amyloid Beta Peptide: A Chemist's Perspective. Role in Alzheimer's and Fibrillization. *Chem. Rev.* **2012**, *112*, 5147−5192.
(30) Castelletto, V.; Edwards-Gayle, C. J. C.; Hamley, I. W.; Barrett, G.; Seitsonen, J.; Ruokolainen, J. Peptide-Stabilized Emulsions And Gels From An Arginine-Rich Surfactant-Like Peptide with Antimicrobial Activity. *ACS Appl. Mater. Interfaces* **2019**, *11*, 9893−9903.
(31) Castelletto, V.; Kaur, A.; Kowalczyk, R. M.; Hamley, I. W.; Reza, M.; Ruokolainen, J. Supramolecular Hydrogel Formation in s Series of Self-Assembling Lipopeptides with Varying Lipid Chain Length. *Biomacromol* **2017**, *18*, 2013−2023.
(32) Levine, H. Thioflavine T Interaction with Synthetic Alzheimer's Disease β-Amyloid Peptides: Detection of Amyloid Aggregation In Solution. *Protein Sci.* **2008**, *2*, 404−410.
(33) Levine, H., Quantification of β-Sheet Amyloid Fibril Structures with Thioflavin T. In *Methods In Enzymology*; Wetzel, R., Ed. Academic Press: San Diego, 1999; Vol. *309*, pp 274−284.
(34) Woody, R. W. Circular Dichroism of Peptides and Proteins. In *Circular Dichroism. Principles And Applications*; Nakanishi, K., Berova, N., Woody, R. W., Eds.; VCH: New York, 1994; pp 473−496.
(35) Bulheller, B. M.; Rodger, A.; Hirst, J. D. Circular snd Linear Dichroism of Proteins. *Phys. Chem. Chem. Phys.* **2007**, *9*, 2020−2035.
(36) Nordén, B.; Rodger, A.; Dafforn, T. R. *Linear Dichroism and Circular Dichroism: A Textbook on Polarized-Light Spectroscopy*; RSC: Cambridge, 2010.
(37) Jackson, M.; Mantsch, H. H. The Use and Misuse of FTIR Spectroscopy in the Determination of Protein Structure. *Crit. Rev. Biochem. Mol. Biol.* **1995**, *30*, 95−120.
(38) Stuart, B. *Biological Applications of Infrared Spectroscopy*; Wiley: Chichester, 1997.
(39) Barth, A. Infrared Spectroscopy of Proteins. *Biochim. Biophys. Acta Bioenerg.* **2007**, *1767*, 1073−1101.
(40) Barth, A. The Infrared Absorption of Amino Acid Side Chains. *Prog. Biophys. Mol. Biol.* **2000**, *74*, 141−173.
(41) Castelletto, V.; Gouveia, R. M.; Connon, C. J.; Hamley, I. W. New RGD- Peptide Amphiphile Mixtures Containing a Negatively Charged Diluent. *Faraday Discuss.* **2013**, *166*, 381−397.
(42) Castelletto, V.; Hamley, I. W., Methods to Characterize the Nanostructure and Molecular Organization of Amphiphilic Peptide Assemblies. In *Peptide Self-Assembly: Methods And Protocols*; Nilsson, B. L., Doran, T. M., Eds.; Humana Press Inc: Totowa, 2018; Vol. *1777*, pp 3−21.
(43) Pabst, G.; Rappolt, M.; Amenitsch, H.; Laggner, P. Structural Information from Multilamellar Liposomes At Full Hydration: Full Q-Range Fitting with High Quality X-Ray Data. *Phys. Rev. E: Stat., Nonlinear, Soft Matter Phys.* **2000**, *62*, 4000−4009.
(44) Serpell, L. C. Alzheimer's Amyloid Fibrils: Structure and Assembly. *Biochim. Biophys. Acta* **2000**, *1502*, 16−30.
(45) Hamley, I. W. Peptide Fibrillisation. *Angew. Chem., Int. Ed. Engl.* **2007**, *46*, 8128−8147.
(46) Ozbas, B.; Kretsinger, J.; Rajagopal, K.; Schneider, J. P.; Pochan, D. J. Salt-Triggered Peptide Folding and Consequent Self-Assembly into Hydrogels with Tunable Modulus. *Macromolecules* **2004**, *37*, 7331−7337.
(47) Jayawarna, V.; Richardson, S. M.; Hirst, A. R.; Hodson, N. W.; Saiani, A.; Gough, J. E.; Ulijn, R. V. Introducing Chemical Functionality in Fmoc-Peptide Gels for Cell Culture. *Acta Biomater.* **2009**, *5*, 934−943.
(48) Adams, D. J.; Mullen, L. M.; Berta, M.; Chen, L.; Frith, W. J. Relationship Between Molecular Structure, Gelation Behaviour and Gel Properties of Fmoc-Dipeptides. *Soft Matter* **2010**, *6*, 1971−1980.
(49) Rodriguez, L. M. D. L.; Hemar, Y.; Cornish, J.; Brimble, M. A. Structure-Mechanical Property Correlations of Hydrogel Forming β-Sheet Peptides. *Chem. Soc. Rev.* **2016**, *45*, 4797−4824.
(50) Scelsi, A.; Bochicchio, B.; Smith, A.; Workman, V. L.; Castillo Diaz, L. A.; Saiani, A.; Pepe, A. Tuning of Hydrogel Stiffness ising a Two-Component Peptide System for Mammalian Cell Culture. *J. Biomed. Mater. Res. A* **2019**, *107*, 535−544.
(51) Guilbaud, J.-B.; Rochas, C.; Miller, A. F.; Saiani, A. Effect Of Enzyme Concentration Of The Morphology and Properties of Enzymatically Triggered Peptide Hydrogels. *Biomacromol* **2013**, *14*, 1403−1411.
(52) Bartucci, M.; Morelli, C.; Mauro, L.; Andò, S.; Surmacz, E. Differential Insulin-Like Growth Factor I Receptor Signaling and Function in Estrogen Receptor (ER)-Positive MCF-7 and ER-Negative MDA-MB-231 Breast Cancer Cells. *Cancer Res.* **2001**, *61*, 6747−6754.
(53) Pozo-Guisado, E.; Alvarez-Barrientos, A.; Mulero-Navarro, S.; Santiago-Josefat, B.; Fernandez-Salguero, P. M. The Antiproliferative Activity of Resveratrol Results in Apoptosis in MCF-7 but not in MDA-MB-231 Human Breast Cancer Cells: Cell-Specific Alteration of The Cell Cycle. *Biochem. Pharmacol.* **2002**, *64*, 1375−1386.
(54) Holliday, D. L.; Speirs, V. Choosing The Right Cell Line for Breast Cancer Research. *Breast Cancer Res.* **2011**, *13*, 7.
(55) Azzam, H. S.; Arand, G.; Lippman, M. E.; Thompson, E. W. Association of MMP-2 Activation Potential with Metastatic Progression in Human Breast-Cancer Cell-Lines Independent of MMP-2 Production. *J. Natl. Cancer Inst.* **1993**, *85*, 1758−1764.
(56) Iyengar, P.; Espina, V.; Williams, T. W.; Lin, Y.; Berry, D.; Jelicks, L. A.; Lee, H.; Temple, K.; Graves, R.; Pollard, J.; Chopra, N.; Russell, R. G.; Sasisekharan, R.; Trock, B. J.; Lippman, M.; Calvert, V. S.; Petricoin, E. F.; Liotta, L.; Dadachova, E.; Pestell, R. G.; Lisanti, M. P.; Bonaldo, P.; Scherer, P. E. Adipocyte-Derived Collagen VI Affects Early Mammary Tumor Progression In Vivo, Demonstrating a Critical Interaction in the Tumor/Stroma Microenvironment. *J. Clin. Invest.* **2005**, *115*, 1163−1176.
(57) Doerr, M. E.; Jones, J. I. The Roles Of Integrins And Extracellular Matrix Proteins in the Insulin-Like Growth Factor I-Stimulated Chemotaxis of Human Breast Cancer Cells. *J. Biol. Chem.* **1996**, *271*, 2443−2447.
(58) Kalyanasundaram, K.; Thomas, J. K. Environmental Effects on Vibronic Band Intensities in Pyrene Monomer Fluorescence and their Application in Studies of Micellar Systems. *J. Am. Chem. Soc.* **1977**, *99*, 2039−2044.
(59) Winnik, F. M. Photophysics of Preassociated Pyrenes in Aqueous Polymer-Solutions and in Other Organized Media. *Chem. Rev.* **1993**, *93*, 587−614.
(60) Zhang, S.; Greenfield, M. A.; Mata, A.; Palmer, L. C.; Bitton, R.; Mantei, J. R.; Aparicio, C.; De La Cruz, M. O.; Stupp, S. I. A Self-Assembly Pathway to Aligned Monodomain Gels. *Nat. Mater.* **2010**, *9*, 594−601.
(61) Boothroyd, S.; Miller, A. F.; Saiani, A. From Fibres to Networks using Self-Assembling Peptides. *Faraday Discuss.* **2013**, *166*, 195−207.
(62) Engler, A. J.; Sen, S.; Sweeney, H. L.; Discher, D. E. Matrix Elasticity Directs Stem Cell Lineage Specification. *Cell* **2006**, *126*, 677−689.

DOI: 10.1021/acsami.9b09065
ACS Appl. Mater. Interfaces 2019, 11, 33573−33580